
Article:
Duckett, Simon orcid.org/0000-0002-9788-6615, Guan, Dexin, Godard, Cyril et al. (3 more authors) (2019) Using Parahydrogen Induced Polarization to Study Steps in the Hydroformylation Reaction. Dalton Transactions. C8DT04723E. ISSN 1477-9234

https://doi.org/10.1039/C8DT04723E

Dalton Transactions

Accepted Manuscript

This article can be cited before page numbers have been issued, to do this please use: D. Guan, C. Godard, A. M. Polas, R. P. Tooze, A. C. Whitwood and S. B. Duckett, *Dalton Trans.*, 2019, DOI: 10.1039/C8DT04723E.

ROYAL SOCIETY OF CHEMISTRY

rsc.li/dalton

ROYAL SOCIETY OF CHEMISTRY View Article Online
DOI: 10.1039/C8DT04723E

Journal Name

ARTICLE

Using *Para*hydrogen Induced Polarization to Study Steps in the Hydroformylation Reaction.

Received 00th January 20xx,
Accepted 00th January 20xx

DOI: 10.1039/x0xx00000x

www.rsc.org/

Dexin Guan,[a,b] Cyril Godard,[b,c] Stacey M. Polas,[d] Robert P. Tooze,[d] Adrian C. Whitwood[b] and Simon B. Duckett[b*]

A range of iridium complexes, Ir(η³-C_3H_5)(CO)(PR_2R')$_2$ (**1a-1e**) [where **1a**, PR_2R' = PPh_3, **1b** P(*p*-tol)$_3$, **1c** $PMePh_2$, **1d** PMe_2Ph and **1e** PMe_3] were synthesized and their reactivity as stoichiometric hydroformylation precursors studied. *Para*-hydrogen assisted NMR spectroscopy detected the following intermediates: Ir(H)$_2$(η³-C_3H_5)(CO)(PR_2R') (**2a-e**), Ir(H)$_2$(η¹-C_3H_5)(CO)(PR_2R')$_2$ (**4d-e**), Ir(H)$_2$(η¹-C_3H_5)(CO)$_2$(PR_2R') (**10a-e**), Ir(H)$_2$(CO-C_3H_5)(CO)$_2$(PR_2R') (**11a-c**), Ir(H)$_2$(CO-C_3H_7)(CO)$_2$(PR_2R') (**12a-c**) and Ir(H)$_2$(CO-C_3H_5)(CO)(PR_2R')$_2$ (**13d-e**). Some of these species exist as two geometric isomers according to their multinuclear NMR characteristics. The NMR studies suggest a role for the following 16 electron species in these reactions: Ir(η³-C_3H_5)(CO)(PR_2R'), Ir(η¹-C_3H_5)(CO)(PR_2R')$_2$, Ir(η¹-C_3H_5)(CO)$_2$(PR_2R'), Ir(CO-C_3H_5)(CO)$_2$(PR_2R'), Ir(CO-C_3H_7)(CO)$_2$(PR_2R') and Ir(CO-C_3H_5)(CO)(PR_2R')$_2$. Their role is linked to several 18 electron species in order to confirm the route by which hydroformylation and hydrogenation proceeds.

Introduction

Gaining a firm understanding of the mode of catalyst action is important when optimal atom efficiency is desired for a transformation. Mechanistic studies underpin this process and normally involve a combination[1-3] of chemical,[4-7] analytical,[8-12] and theoretical work.[13-19] *In situ* NMR methods are gaining in importance[1, 20-24] in this regard despite the techniques inherent low sensitivity. This change is a result of improved hardware,[25] novel *in situ* high pressure methods[20, 21, 26] and *in situ* photochemical approaches,[27, 28] with hyperpolarization methods in the solid and solution phases adding a further level of refinement.[23, 24]

Hydroformylation reflects a widely used industrial reaction that converts a range of alkenes into aldehydes, esters and other important chemical feedstocks.[29-32] In hydroformylation, both linear and branched products form and their ratio is an important parameter in maximising commercial return.[33, 34] While many experimental and theoretical studies have been undertaken to probe hydroformylation, most have been based on cobalt[35-39] or rhodium.[40-43] Surprisingly, iridium[44] has been shown to transform 1-hexene and 1-octene with an activity that is just 8 times slower[45, 46] than that seen for rhodium. However, hydrogenation, as a side reaction, leads to reduced atom efficiency.[47] Both CO and PPh_3 ligand exchange processes at rhodium have been explored by Brown and co-workers using $RhH(CO)(PPh_3)_3$ that underpin its role in hydroformylation[6] and studies on related phosphine and phosphite based systems have also been undertaken for related hydride, alkyl, allyl and acyl substituted complexes.[48, 49] Such species are often more stable for iridium which therefore reflects a good starting point from which to study this reaction.[50, 51] This is reflected in the fact that Ir(CO-Et)(H)$_2$(dppe)(CO) and Ir(CO-Et)(H)$_2$(Xantphos)(CO) have been isolated and characterised by Eisenberg.[52] In fact, one of the earliest mechanistic studies on hydroformylation using nuclear magnetic resonance (NMR) spectroscopy involved Ir(η³-C_3H_5)(CO)(PPh_3)$_2$.[5] In this case, Ir(η¹-C_3H_5)(CO)$_2$(PPh_3)$_2$ and Ir(CO-η¹-C_3H_5)(CO)$_2$(PPh_3)$_2$ were isolated.

Earlier studies in our group used an array of Co(η³-C_3H_5)(CO)$_2$(phosphine) complexes in conjunction with the *para*-hydrogen induced polarization (PHIP) effect to assist in the NMR spectroscopy examination of hydroformylation.[24, 55] We employ the PHIP effect here to detect further species in this iridium study. This works because when *p*-H_2 is introduced into a material, the resulting PHIP effect facilitates the detection of low concentration reaction intermediates, whilst also provides a route to obtain additional kinetic information on their role in a reaction.[53,54] In the case of Co(η³-C_3H_5)(CO)$_2$(PPh_3), harnessing the unsaturated allyl centre as a *p*-H_2 acceptor allows the intermediates Co(C_3H_7)(CO)$_2$(PPh_3) and Co(CO-C_3H_7)(CO)$_2$(PPh_3) to be detected and characterized by NMR methods during catalysis through a PHIP response.[24, 55] Interestingly at higher temperatures, rapid equilibration

[a] School of Innovation and Entrepreneurship, Zhejiang University of Science and Technology, Hangzhou, Zhejiang Provence, China. 310023
[b] Department of Chemistry, University of York, Heslington, York, YO10 5DD, UK.
[c] Departament de Química Física i Inorgànica, Universitat Rovira I Virgili, C/Marcel.li Domingo s/n, 43007 Tarragona, Spain
[d] Sasol Technology, St Andrews, Scotland, UK

Electronic Supplementary Information (ESI) available: [details of any supplementary information available should be included here]. See DOI: 10.1039/x0xx00000x

between a number of reaction intermediates suggested that the linear to branched product ratio was controlled by thermodynamic stability. As PHIP enables the detection of scalar coupled heteronuclei through polarisation transfer the reliable characterisation of such species can be achieved.[56] This method has also been used to examine a range of heterogeneous reactions[57-61] and some that don't involve a metal centre.[62-65] It has therefore developed substantially from the starting point of Weitekamp,[66, 67] Eisenberg[68, 69] and Bargon,[70, 71] and has been reviewed.[72-74] Here the reactivity of $Ir(\eta^3\text{-}C_3H_5)(CO)(PR_2R')_2$ (**1a**-**1e**) [where PR_2R' is PPh_3 (**1a**), P(*p*-tol)$_3$ (**1b**), $PMePh_2$ (**1c**), PMe_2Ph (**1d**) and PMe_3 (**1e**)] towards CO and *p*-H_2 is examined and a number of new species characterised.

Results and discussion

Synthesis and characterisation of $Ir(\eta^3\text{-}C_3H_5)(CO)(PR_2R')_2$ (1a-1e)

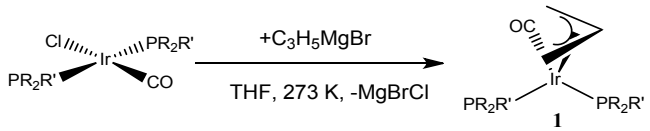

Scheme 1 Synthesis of **1a**-**1e**, where PR_2R' is PPh_3 (**1a**), P(*p*-tol)$_3$ (**1b**), $PMePh_2$ (**1c**), PMe_2Ph (**1d**) and PMe_3 (**1e**).

The synthesis of complexes **1a**-**1e** was achieved according to Scheme 1. This reaction involves the addition of allyl magnesium bromide to the appropriate analogue of Vaska's complex $IrCl(CO)(PR_2R')_2$ in THF.[5, 75-77] The ^1H and ^{31}P NMR spectra of the crude reaction products obtained for **1a** and **1b** revealed the formation of *ca.* 15 % of the side-products $IrH(CO)(PPh_3)_3$ and IrH(CO)(P-*p*-toly$_3$)$_3$ respectively, whereas **1c**-**1e** formed in sufficient purity for further NMR study without further separation. Purification of **1a** and **1b** was achieved though by washing the crude product with pentane under an inert atmosphere. Subsequently, **1a**-**1e** were characterised by multinuclear NMR spectroscopy, as detailed in the ESI. In addition, crystals of **1a**, $Ir(\eta^3\text{-}C_3H_5)(CO)(PPh_3)_2$[23] and **1b**, Ir($\eta^3$-$C_3H_5$)(CO)(P-*p*-tolyl$_3$)$_2$ that were suitable for X-ray crystallography were grown from diethyl ether at room temperature while crystals of $IrH(CO)(PPh_3)_3$ were obtained from pentane. The structures of **1a** and **1b** are illustrated in Fig. 1 while that of $IrH(CO)(PPh_3)_3$ is presented in the ESI.

(a) (b)

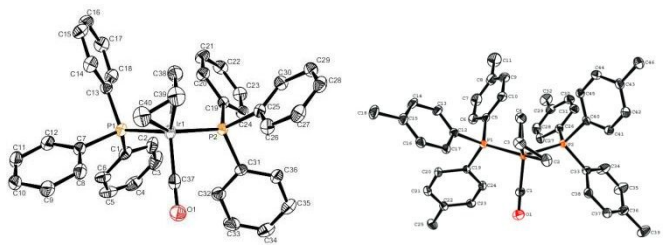

Fig. 1 ORTEP diagrams of (a) $Ir(\eta^3\text{-}C_3H_5)(CO)(PPh_3)_2$ (**1a**) and (b) Ir(η^3-C_3H_5)(CO)(P(*p*-tolyl)$_3$)$_2$ (**1b**), with ellipsoids drawn at 50 % probability level.

These structures reveal that **1a** and **1b** adopt distorted piano-stool geometries with capping η^3-allyl ligands in a similar arrangement to that seen in a range of related complexes.[78, 79] The structures are very similar to each other with the Ir-P distances of **1a** and **1b** being close (see Tables 1 and 2). The increase in electron density resulting from moving from PPh_3 to P(p-tolyl)$_3$ is insufficient to change the Ir-C(O) bond length in **1a** from that in **1b**. However, the Ir-C_{allyl} bond lengths of **1a** are slightly longer than those of **1b**. These observations suggest that the iridium centre of **1b** is indeed more electron rich than that of **1a** because of the stronger Ir-allyl interaction.

Table 1 Selected bond lengths (Å) and angles (°) for **1a**

Ir(1)-P(2)	2.2953(7)	Ir(1)-C(40)	2.209(3)
Ir(1)-P(1)	2.3456(7)	C(37)-O(1)	1.159(4)
Ir(1)-C(37)	1.862(3)	C(38)-C(39)	1.440(5)
Ir(1)-C(39)	2.127(3)	C(39)-C(40)	1.422(5)
Ir(1)-C(38)	2.204(3)	C(37)-Ir(1)-P(2)	92.47(8)
P(2)-Ir(1)-P(1)	112.79(3)	C(40)-C(39)-C(38)	113.3(3)
C(37)-Ir(1)-P(1)	100.79(9)	O(1)-C(37)-Ir(1)	178.7(2)
C(37)-Ir(1)-C(40)	98.90(13)	C(37)-Ir(1)-C(39)	117.28(14)
C(39)-Ir(1)-C(40)	38.24(12)	C(37)-Ir(1)-C(38)	155.14(13)
C(38)-Ir(1)-C(40)	65.62(13)	C(39)-Ir(1)-C(38)	38.81(13)

Table 2 Selected bond lengths (Å) and angles (°) for **1b**

Ir(1)-C(1)	1.861(4)	Ir(1)-P(2)	2.3520(10)
Ir(1)-C(3)	2.120(5)	O(1)-C(1)	1.161(6)
Ir(1)-C(2)	2.189(5)	C(2)-C(3)	1.445(7)
Ir(1)-C(4)	2.194(5)	C(3)-C(4)	1.448(7)
Ir(1)-P(1)	2.2952(12)	C(2)-C(3)-C(4)	113.1(4)
C(1)-Ir(1)-C(3)	115.7(2)	O(1)-C(1)-Ir(1)	176.3(4)
P(1)-Ir(1)-P(2)	112.02(4)	C(1)-Ir(1)-C(2)	96.0(2)
C(1)-Ir(1)-P(2)	103.20(14)	C(3)-Ir(1)-C(4)	39.18(19)
C(1)-Ir(1)-P(1)	94.88(15)	C(1)-Ir(1)-C(4)	154.2(2)
C(2)-Ir(1)-C(4)	66.8(2)	C(3)-Ir(1)-C(2)	39.14(19)

Fluxional behaviour of $Ir(\eta^3\text{-}C_3H_5)(CO)(PR_2R')_2$ (1a-1e)

Fluxionality in the ^1H NMR spectrum of **1a** has been described previously.[5] However modern NMR methods offer the opportunity to re-examine this property at higher field. We obtained kinetic information on this process by EXSY methods. We first describe the temperature dependence of the NMR signals that are seen for **1a** and **1e** before detailing these results.

Two broad multiplets at δ 1.18 (*syn*) and δ 2.44 (*anti*) are seen alongside a sharper multiplet at δ 4.32 (*meso*) for the η^3-allyl ligand in the 400 MHz ^1H NMR spectrum of **1a,** recorded in d_8-toluene at 295 K. Upon cooling to 203 K, both the δ 1.18 and the δ 2.44 signals split into two as the four methylene protons of the η^3-allyl ligand become inequivalent. In contrast, the only ally ligand signal for **1e** that is visible at 295 K corresponds to that of the H_{meso} resonance, the methylene protons remaining invisible until 233 K is reached. Now 2D-

COSY experiments located two signals at δ 2.76 and δ 1.08 for the H_{syn} and H_{anti} resonance of **1e**, which split into four signals at δ 2.90, 1.70, 1.17 and 0.62 when the sample is cooled further to 203 K. Similar effects have been seen with ($^{t\text{-}Bu}$POCOP)Ir(η^3-C_3H_5)(H).[80]

This behaviour can also be viewed in the corresponding ^{31}P[20] NMR spectra which change from a single broad peak at δ −57.5 and 295 K, to two mutually coupled signals at δ −52.1 and δ −59.3 and 203 K in the case of **1e**. These observations match those previously reported for Ir(η^3-C_3H_4Ar)(CO)(PPh_3)$_2$.[81] The inequivalence of these groups, as revealed by these NMR data, is matched by the solid state structures shown in Fig. 1.

The process by which the proton and phosphorus sites interconvert was monitored by EXSY spectroscopy between 193 K and 223 K for **1a**. Identical rates of site interchange were obtained for the two different nuclei by simulation, and the associated activation *para*meters were determined to be: $\Delta H^{\neq}$ = 34 ± 1 kJ mol^{-1}, $\Delta S^{\neq}$ = -43 ± 3 J mol^{-1} K^{-1} and $\Delta G^{\neq}_{203K}$ = 44.2 ± 0.5 kJ mol^{-1} (see ESI). These results are detailed in Table 3. This process proved to be unaffected by the addition of pyridine and hence we can rule out the involvement of an η^1-allyl intermediate. The negative entropy of activation suggests that the interchange process simply corresponds to η^3-allyl rotation as described in **Scheme 1**.

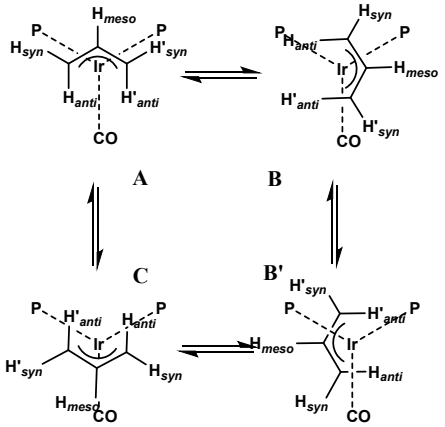

Scheme 1 Mechanism of ally-proton and phosphorus ligand exchange as seen for complexes **1a**-**1e** by NMR.

1b-**1e** show similar fluxional behaviour according to our NMR studies. The kinetics of the corresponding rotations in **1b**-**1e** were determined by monitoring the corresponding ^{31}P NMR changes from 203 K to 293 K. Results for these processes are summarized in the ESI and Table 3.

The free energy barriers to η^3-allyl rotation at 203 K were found to decrease in the order PPh_3 ~ $PMePh_2$ > P-(*p*-tol)$_3$ > PMe_2Ph > PMe_3 and follow the electron donating power of the phosphine.[82] Unfortunately, the corresponding $\Delta H^{\neq}$ values are not clearly differentiated, although that for PMe_3 is larger than that for PPh_3, while the $\Delta S^{\neq}$ values suggest that bulkier PPh_3 involves a more ordered transition state than smaller PMe_3. As no clear trend is evident in these data, we conclude that both steric and electronic effects must play their part in contributing to the activation barrier for this process.

Table 3 Activation parameters for **1a**-**1e**, as determined from a series of ^{31}P{^{1}H} NMR spectra between 203 K and 293 K

Species	$\Delta H^{\neq}$ (kJ mol^{-1})	$\Delta S^{\neq}$ (J mol^{-1} K^{-1})	$\Delta G^{\neq}$ 203 K (kJ mol^{-1})
1a	34 ± 1	-43 ± 3	44.2 ± 0.05
1b	31 ± 3	-63 ± 14	43.3 ± 0.05
1c	41 ± 2	-14 ± 10	44.2 ± 0.05
1d	33 ± 6	-46 ± 14	43.0 ± 0.05
1e	39 ± 2	-14 ± 6	42.2 ± 0.05

Reactivity of 1a-1e towards H_2 at low temperature: detection of Ir(H)$_2$(CO)(PR$_2$R')(η^3-C_3H_5).

We then examined the addition of *p*-H_2 to a series of NMR samples of **1b**-**1e**. The reactions involving **1a** and **1b** were initially undertaken at 273 K, while that for **1c** employed 253 K, that for **1d** 233 K and that for **1e** 203 K. This change in temperature reflects the different reactivity of these complexes and we note that by subsequently varying the temperature we detect an array of PHIP enhanced hydride signals for several reactions intermediates that lie on the pathway to formation of the corresponding *fac* and *mer* isomers of Ir(H)$_3$(CO)(PR$_2$R')$_2$.

Initially, all of these reactions with H_2 proceed to form two isomers of Ir(H)$_2$(CO)(PR$_2$R')(η^3-C_3H_5) (**2**$_A$ and **2**$_B$) as detailed in the ESI and Table 4. These complexes are not stable and maintain their PHIP enhancements for long periods of time as the H_2 addition step is reversible. When these reactions are examined under normal hydrogen these products are not visible due to the fact that these reaction products are only formed in small amounts. Additionally, the observation that the formation of both isomers is suppressed by the addition of phosphine (PR$_2$R') suggests they result from the corresponding 16-electron phosphine loss products according to Scheme 2.

Table 4 Comparison of the ratios of **2**$_A$ and **2**$_B$ that are formed when **1a**-**1e** react with *p*-H_2 at the indicated temperature, and the steric and electronic properties of the corresponding phosphine ligand[82]

Species	Ratio	cone angle	υ_{CO} (cm^{-1}) for Ni(PR$_2$R')(CO)$_3$
2a$_A$: **2a**$_B$ (273 K)	1:1.8	145	2068.9
2b$_A$: **2b**$_B$ (273 K)	1:1.7	145	2066.7
2c$_A$: **2c**$_B$ (253 K)	1:1.5	136	2067.0
2d$_A$: **2d**$_B$ (233 K)	1 :1	122	2065.3
2e$_A$: **2e**$_B$ (203 K)	1: 0.6	118	2064.1

We start by describing these observations in more detail for complex **1e** because this reaction proceeds clearly at 203 K and provides some of the most interesting and readily understandable observations. In fact, the PHIP enhanced signals for the hydride resonances of **2e** appear with the strongest signal intensities when these systems are compared. The hydride signals of the two mono phosphine products **2e**$_A$ and **2e**$_B$ are, however, complicated by resonance overlap unless ^{31}P decoupling is applied. This overlap is detailed in Fig. 2. The hydride signal of **2e**$_A$, at δ −11.7 (H_b), exhibits a *trans* J_{HC} coupling of 45.2 Hz when ^{13}CO is employed, and both it, and its partner that appears at δ -11.4 (H_a) exhibits a single *cis*

View Article Online
DOI: 10.1039/C8DT04472F

phosphorus coupling. In contrast, the hydride signal of **2e$_B$** which appears at δ −11.6 (H$_d$), possesses a large *trans* J_{HP} coupling of 148 Hz while its partner at δ −12.0 (H$_c$) exhibits a *cis* J_{HP} coupling of 16 Hz, in addition to the J_{HH} splitting of −6 Hz which both hydride ligands experience. These characteristics differentiate the ligand arrangements of these isomeric products, as detailed in Scheme 3, and it is notable that the ratio of the hydride ligand signals for **2e$_A$**:**2e$_B$** at 203 K is 5:3. Table 4 presents the corresponding signal intensity ratios that were observed for the analogous **A** and **B** isomers of **2b**-**2e** at the indicated temperatures (see ESI and Table 5 for more details). It is clear that, as expected, when the electron donating power of the phosphine increases,[82, 83] H_2 addition over the CO-Ir-C axis of the intermediate Ir(η^3-C_3H_5)(CO)(PR$_2$R')$_2$ becomes favoured.[84]

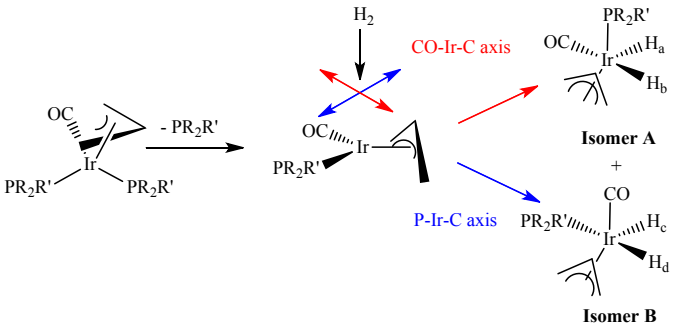

Scheme 2 The reaction of **1a**-**1e** with H_2 at leads to two isomeric forms of Ir(H)$_2$(CO)(PR$_2$R')(η^3-C_3H_5) (**2$_A$** and **2$_B$**) after phosphine loss whose ratio depends on the identify of PR$_2$R'.

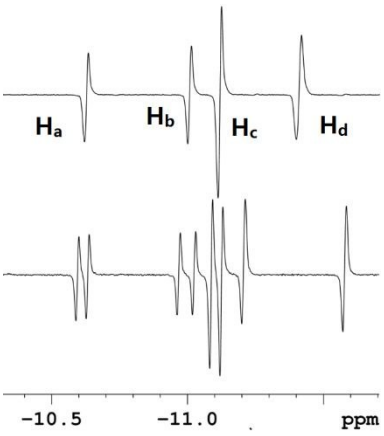

Fig. 2 ^{1}H (lower) and ^{1}H{^{31}P} (upper) NMR spectra detailing the hydride region under PHIP enhancement during *p*-H_2 addition to **1e** at 203 K. Signals for **2e$_A$** and **2e$_B$** are indicated using the labels H$_a$-H$_d$ as described in the text and Scheme 3.

Reactivity of 1e towards H_2 at 233 K: detection of Ir(H)$_3$(CO)(PMe$_3$)$_2$ (3e$_F$ and 3e$_M$) and Ir(H)$_2$(η^1-C_3H_5)(CO)(PMe$_3$)$_2$

We then re-examined the reaction of **1e** with *p*-H_2 at 233 K. Now stronger PHIP can be seen in the corresponding hydride ligand signals for **2e$_A$** and **2e$_B$**. However, removing this cold NMR sample from the NMR spectrometer and rapidly shaking it at room temperature before returning it to the cold NMR probe as series of changes become evident. These correspond to the observation of a number of additional PHIP enhanced hydride ligand signals as shown in Fig. 3b and 3c. Interestingly, when the sample has cooled back to 233 K, only the signals for **2e$_A$** and **2e$_B$** remain strongly polarised (Fig. 3d). This confirms the reversibility of the H_2 addition step that forms them and suggests that the other species are produced at higher temperature. Based on the earlier work of Wilkinson we expected to see evidence for the *fac* and *mer* isomers of Ir(H)$_3$(CO)(PMe$_3$)$_2$ (**3e$_F$** and **3e$_M$**) amongst these signals and we now consider these changes for the **1e** system in more detail before considering those seen with the other complexes.[5]

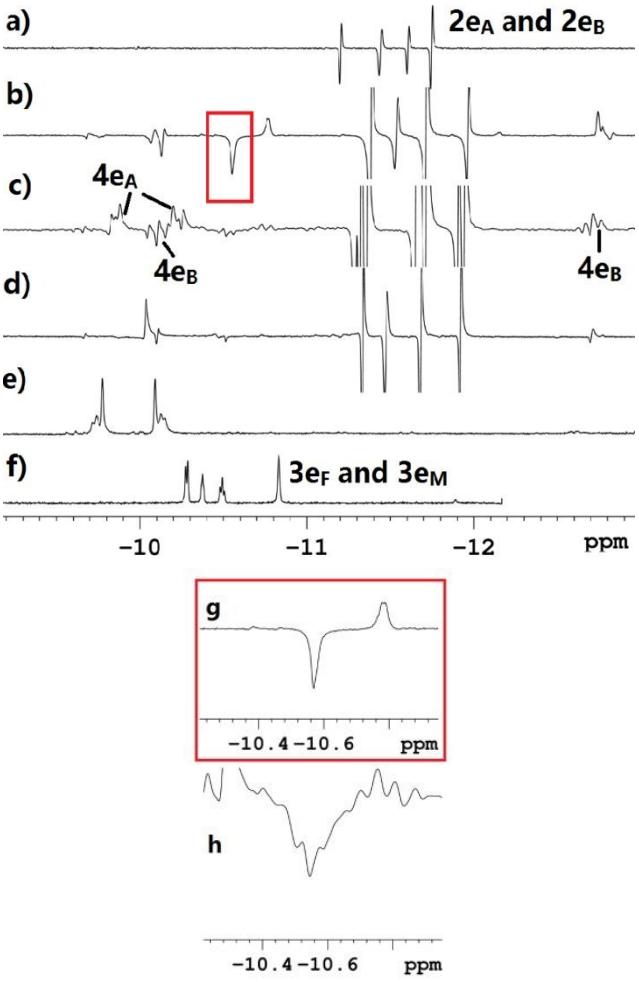

Fig. 3 Hydride region of a series of ^{1}H NMR spectra (a)-(h) that were recorded when **1e** reacts with *p*-H_2 under the indicated conditions. a) Reference spectrum showing signals for **2a$_A$** and **2a$_B$** at 203 K; b) ^{1}H{^{31}P} trace at 233 K, recorded immediately after shaking and reintroduction; c) corresponding ^{1}H trace; d) ^{1}H{^{31}P} trace one hour later; e) ^{1}H trace 12 hours later; f) ^{1}H NMR reference showing signals for **3e$_F$** and **3e$_M$** at 298 K; g) expansion of the ^{1}H{^{31}P} result for the hydride signal of HIr(CO)(PMe$_3$)$_2$ and h) expansion of the ^{1}H trace of the hydride signal for HIr(CO)(PMe$_3$)$_2$. Red box identifies the region used in the expansion.

Firstly, we note that the additional signal at δ −10.0 of Fig. 3 is diagnostic of an [AX]$_2$ spin system and is therefore associated with the formation of a dihydride complex which contains an Ir(H)$_2$(PMe$_3$)$_2$ core where $|J_{HP(trans)}+J_{HP(cis)}|$ is 126 Hz. Consequently, if this species is formed from **2e**, rebinding of the initially liberated PMe$_3$ is required. A single ^{31}P environment was detected at δ −57.9 for this product through

View Article Online
DOI: 10.1039/C8DT04723E

HMQC methods and further characterization was achieved by successful nOe transfer from the hydride ligand signal to a δ 1.26 signal for bound PMe_3, with additional peaks being detected at δ 1.95 (J_{HP} = 6.6 and J_{HH} = 7 Hz), 4.60, 4.76 and 6.94 due to an η^1-$CH_2CH{=}CH_2$ group. This reaction product therefore corresponds to $Ir(H)_2(\eta^1\text{-}C_3H_5)(CO)(PMe_3)_2$ (**4e$_A$**) and reflects an intermediate that forms on the route to **3** and propene/propane. Its formation from **2** would be expected to occur after η^3-η^1 allyl rearrangement.

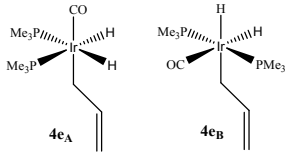

Fig. 4 Ligand arrangements within $Ir(H)_2(\eta^1\text{-}C_3H_5)(CO)(PMe_3)_2$ (**4e$_A$** and **4e$_B$**).

The formation of a second isomer of **4e$_A$**, **4e$_B$** was confirmed in a further series of measurements (Fig. 4). This second species yields two antiphase hydride signals at δ −12.67 and δ −10.06 which both contain *cis* couplings to two equivalent phosphorus centres that were shown to resonate at δ −47.2; the latter hydride signal overlaps with the unique signal of **4e$_A$** but its presence can be readily seen in the fully coupled ^{1}H NMR spectrum (Fig. 3c). The ratio of **4e$_A$** to **4e$_B$** proved to be 1:1.4 according to the observed signal intensities, but these signals are over 20 times smaller than those of **2e$_A$**. We note that **4e$_A$** is thermally stable (Fig. 3e) while **4e$_B$** is only seen through the PHIP effect.

A further hydride resonance is observed in these ^{1}H NMR spectra as an emission signal at ~δ −10.56 which possesses a triplet multiplicity in a fully coupled proton spectrum where J_{PH} is 16 Hz. This resonance is detected through the one-proton PHIP effect of Eisenberg[52] and arises from a monohydride complex, most likely $HIr(CO)(PMe_2)_2$, or its solvent adduct, that results from the loss of propene from **4e**. The observation of a signal with these characteristics has been suggested to originate in a second order spin system as exemplified by **4**. Its observation here therefore corresponds to the detection of a reaction intermediate that lies on the route to the final reaction product, the trihydride, $Ir(H)_3(CO)(PMe_3)_2$ which exists in *fac* (**3e$_F$**) and *mer* (**3e$_M$**) forms (Fig 3f). Furthermore, when such a sample is kept at 233 K without warming, **4e$_A$** becomes the dominant species in solution, and upon warming the sample to 298 K propane readily forms alongside the two trihydride products **3e$_M$** and **3e$_F$**. We have therefore detailed a series of observations that map the conversion of **1e** into **3e**.

Reactivity of 1a-1d towards H_2 at moderate temperatures

Similar observations were made when the reaction with **1d** was examined at 233 K (see ESI and Table 5 and 6 for details). When, however, the analogous reaction with **1b** is monitored at 273 K, resonances of **2b$_A$** and **2b$_B$** are readily seen alongside signals for **3b$_M$** at δ −9.25 and δ −9.89 (Fig. 5a and Table 6). This higher temperature is needed to facilitate the initial detection of **2** and logically reflects the point at which **1b** undergoes phosphine loss. Unfortunately, **2** is then highly reactive, and while the intensity difference between the hydride signals of **2b$_A$** and **3b$_M$** is 7 fold in favour of the former

Table 5 Multinuclear NMR data for the two isomers of the allyl dihydride complexes $Ir(H)_2(CO)(PR_2R')(\eta^3\text{-}C_3H_5)$ (**2a**-**2e**) of Scheme 3, couplings in Hz.

Complex	Temperature /K	^{1}H, δ, hydride (multiplicity)	^{13}C{^{1}H}, δ, CO	^{31}P{^{1}H}, δ, PR_2R'
2a$_A$	273	−10.8, dd, J_{PH} = 15, J_{HH} = -5, H_a −11.2, dd, J_{PH} = 25, J_{HH} = -5, H_b	174.7 [a], d, J_{PC} = 9	14.00, (s)
2a$_B$		−11.3, dd, J_{PH} = 16, J_{HH} = -5, H_c −11.6, dd, J_{PH} = 151, J_{HH} = -5, H_d	175.5 [a], d, J_{PC} = 8	3.77, (s)
2b$_A$	273	−11.2, dd, J_{PH} = 23, J_{HH} = -4, H_a −10.6, dd, J_{PH} = 15, J_{HH} = -4, H_b	176.4 [a] (d, J_{PC} = 5)	11.2 (s)
2b$_B$		−11.1, dd, J_{PH} = 15, J_{HH} = -5, H_c −11.4, dd, J_{PH} = 149, J_{HH} = -5, H_d	178.2 [a] (d, J_{PC} = 5)	1.9 (s)
2c$_A$	253	−11.0, dd, J_{PH} = 16, J_{HH} = -5, H_a −11.5, dd,J_{PH} = 24, J_{HH} = -4, H_b	175.3 [a] (d, J_{PC} = 5)	−11.3 (s)
2c$_B$		−11.6, dd, J_{PH} = 17, J_{HH} = -4, H_c −11.3, dd, J_{PH} = 150, J_{HH} = -4, H_d	175.5 [a] (d, J_{PC} = 6)	−15.7 (s)
2d$_A$	273	−11.2, dd, J_{PH} = 12, J_{HH} = -5, H_a −11.6, dd, J_{PH} = 17, J_{HH} = -5, H_b	---[b]	−32.8 (s)
2d$_B$		−11.4, dd, J_{PH} = 18, J_{HH} = -4, H_c −11.7, dd, J_{PH} = 148, J_{HH} = -4, H_d	---[b]	−39.5 (s)
2e$_A$	233	−11.4, dd, J_{PH} = 17, J_{HH} = -7, H_a −11.7, dd, J_{PH} = 24, J_{HH} = -7, H_b	175.6[c] (d, J_{PC} = 6)	−47.47 (s)
2e$_B$		−12.00, dd, J_{PH} = 16, J_{HH} = -6, H_c −11.60, dd, J_{PH} = 148, J_{HH} = -6, H_d	175.8[c] (d, J_{PC} = 6)	−56.97 (s)

a): detected when the reaction of **1a-c** with ^{13}COand *p*-H_2 is undertaken; b): not detect due to unsuccessful labelling, see ESI for details; c): detected using ^{13}CO enriched **1e**

View Article Online
DOI: 10.1039/C8DT04723E

the reaction system is no longer stable. Furthermore, product **4b**, is much harder to detect than was the case for **1e** because of the higher temperatures needed. These effects are portrayed in the series of NMR spectra that are illustrated in Fig. 5.

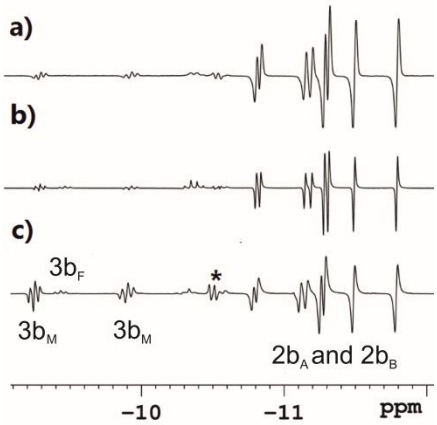

Fig. 5 Hydride region of a series of ^{1}H NMR spectra (a)-(c) that were recorded as **1d** reacts with *p*-H_2 at (a) 273 K, (b) 283 K and (c) 298 K. Signals for **2b$_A$**, **2b$_B$**, **3b$_F$** and **3b$_M$** are indicted. *is unassigned and due to a dihydride species that yields signals at δ −10.48 (J_{PH} = 18 Hz) and δ −13.25 (J_{PH} = 137.7 Hz) and contains a single phosphine ligand.

By comparison to the 273 K data, at 283 K the PHIP enhanced NMR signals all grow in relative intensity, while those for **3b$_F$** ultimately appear without polarisation as it now accumulates to the point it is seen as a stable product. At 298 K, strongly polarised signals for the hydride ligands of **3b$_M$** are seen alongside weak signals for **3b$_F$** which do not exhibit PHIP. The ratio of the *fac* and *mer* products proved to be 1:2.6 in the early stages of this reaction, however, when the sample was warmed to 373 K, and cooled back to 298 K, the ratio of **3b$_M$** : **3b$_F$** changed to 1:1.2. Hence we can conclude the formation of **3b$_M$** is kinetically favoured.[84] The ESI contains the associated NMR data for the corresponding reaction with **1a**. These data reveal that the ratio of the *mer* and *fac* isomers changes with phosphine such that the *fac* isomer is favoured for PMe_3 in accordance with its high electron donating power and small size. Equilibria between **3a$_M$** and **3a$_F$** have been explored recently using FTIR and *in-situ* high pressure NMR methods.[85]

Reactivity of 1 towards H_2 at 298 K

We then prepared a further series of samples of **1a**-**1e** and monitored their reaction with *p*-H_2 at 298 K. Collectively, while good PHIP enhancements were seen for the hydrogenation product propane at δ 0.9 and δ 1.34 in the corresponding ^{1}H NMR spectra they were far more limited for propene (Fig. 6).

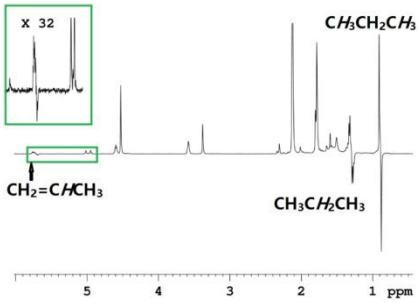

Fig. 6 Typical ^{1}H NMR spectrum showing the organic region that is observed when **1c** reacts with *p*-H_2 at 298 K. The PHIP enhanced signals of propene and propane are indicated.

Table 6 Multinuclear NMR data for the *fac* and *mer* isomers of $Ir(H)_3(CO)(PR_2R')_2$ (**3**) that are produced by the reaction of **1a**-**1e** with *p*-H_2 at the indicated temperature with their relative proportions, couplings in Hz.

Species	*fac* : *mer* ratio	temperature /K	^{1}H (δ) multiplicity and couplings at 298 K		^{31}P{^{1}H}, δ
3a	6 : 1	298	**3a$_f$**	−9.3 (1H, tt, J_{PH} = 16.8, J_{HH} = −4.5) −10.8 (2H, m, $\|J_{HP(trans)} + J_{HP(cis)}\|$ = 107)	16.9
	1.4 : 1	363	**3a$_m$**	−10.0 (2H, dt, J_{PH} = 19.5, J_{HH} = −4.4) − 9.5 (1H, tt, J_{PH} = 18, J_{HH} = -4.4)	7.8
3b	2.6 : 1	298	**3b$_f$**	−9.4 (1H, tt, J_{PH} = 18.8, J_{HH} = −4.5) −10.4 (2H, m, $\|J_{HP(trans)} + J_{HP(cis)}\|$ is 106)	-
	1.2 : 1	363	**3b$_m$**	−9.3 (2H, dt, J_{PH} = 16.7, J_{HH} = −4.5) − 9.9 (1H, tt, J_{PH} = 20, J_{HH} = −4.5)	13.8
3c	3.7 : 1	298	**3c$_f$**	−10.1 (1H, tt, J_{PH} = 21, J_{HH} = −3.3) −10.6 (2H, m, $\|J_{HP(trans)} + J_{HP(cis)}\|$ = 107)	-
	3.7 : 1	363	**3c$_m$**	−9.8 (2H, dt, J_{PH} = 16.8, J_{HH} = −4.6) −10.6 (1H, tt, J_{PH} = 20.8, J_{HH} = −4.6)	−18.3
3d	3.8 : 1	298	**3d$_f$**	−10.3 (1H, tt, J_{PH} = 21.4, J_{HH} = −5 z) −11.0 (2H, m, $\|J_{HP(trans)} + J_{HP(cis)}\|$ = 104)	−41.3
	3.8 : 1	363	**3d$_m$**	−10.2 (dt, J_{PH} = 17, J_{HH} = −4.6) −10.7 1H, tt, J_{PH} = 21, J_{HH} = −5)	−30.2
3e	1.05 : 1	298	**3e$_f$**	−10.4 (1H, tt, J_{PH} = 21, J_{HH} = −3.3) −10.8 (2H, m, $\|J_{HP(trans)} + J_{HP(cis)}\|$ = 102)	−59.3
	1.05 : 1	363	**3e$_m$**	−10.3 (2H, dt, J_{PH} = 17, J_{HH} = −4.0) −10.5 (1H, tt, J_{PH} = 20, J_{HH} = −4.0)	−49.6

View Article Online
DOI: 10.1039/C8DT04723E

This indicates that when pairwise hydride migration from a single *p*-H_2 molecule into the η^3-allyl ligand proceeds to form propane, it is effectively irreversible. We note that the corresponding cobalt[24, 55] complexes yield strong PHIP polarisation in the ^{1}H NMR signals of propene during analogous measurements which now indicate a high level of reversibility in the hydride transfer step. This process is needed in order to place two protons from a single *p*-H_2 molecule into a single molecule of propene. As expected, signals for **3** were also visible under these conditions.

Reactivity of 1a-1d towards CO

Before studying the reaction of **1a-1e** with CO and H_2 we examined their reactions with CO alone. We first looked at **1a** at 298 K and observed the facile formation of a mixture of $Ir(\eta^3\text{-}C_3H_5)(CO)_2(PPh_3)$ (**5a**), $Ir(CO)_3(PPh_3)(\eta^1\text{-}CH_2CH{=}CH_2)$ (**6a**), $Ir(CO)_3(PPh_3)(COCH_2{=}CHCH_2)$ (**7a**) and $Ir(CO)_2(PPh_3)_2(COCH_2CH{=}CH_2)$ (**8a**). These observations match with those of Wilkinson and confirm that the reactions with both CO and PPh_3 are highly reversible.[5, 6] The proportion of these species is highly dependent on the CO pressure and the reaction time. Complexes **1b**-**1c** proved to show similar reactivity and NMR data for the corresponding species detected in this study are detailed in the ESI.

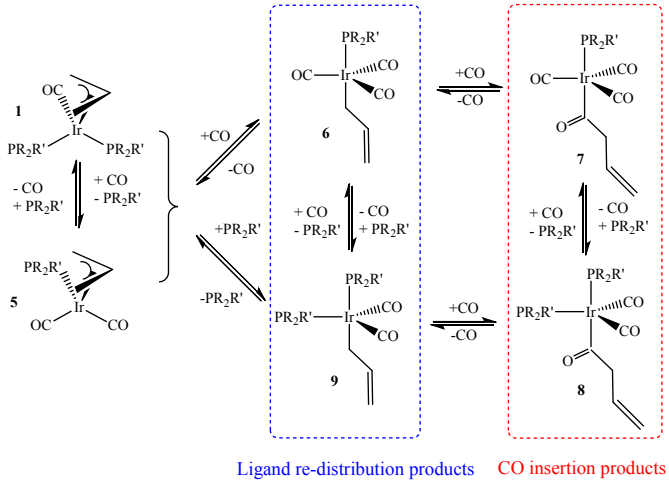

Scheme 4 Reactivity of **1a-1e** towards CO, proportions differ according to PR_2R'

When a sample of **1e** was exposed to CO at 203 K, the only detected product corresponds to **9e**, $Ir(CO)_2(PMe_3)_2(\eta^1\text{-}CH_2CH{=}CH_2)$. This complex yields two ^{31}P signals at δ -63.3 and δ -53.9 and a ^{13}C CO signal at δ 190.5, as detailed in Fig. 7. When ^{13}CO was used, additional J_{PC} couplings were seen of 32 and 11 Hz respectively. **9e** remained dominant up to 263 K, under CO (or synthetic gas), but beyond this point, the formation of the analogous complexes **6e**, **7e** and **8e** were indicated. The analogous reaction with **1d** at 203 K again led selectively to **9d** but when **1c** was examined, **9c** and **6c** proved to form in the ratio 12:1 at 203 K. Consequently, we examined the reactions of **1a** and **1b** at 203 K and observed the formation of **5** and **6**, in a ratio of 2:1 in both cases. **9** was not seen to form and hence the identity of the phosphine used in these reactions introduces an element of selectivity. These results are detailed in Scheme 4.

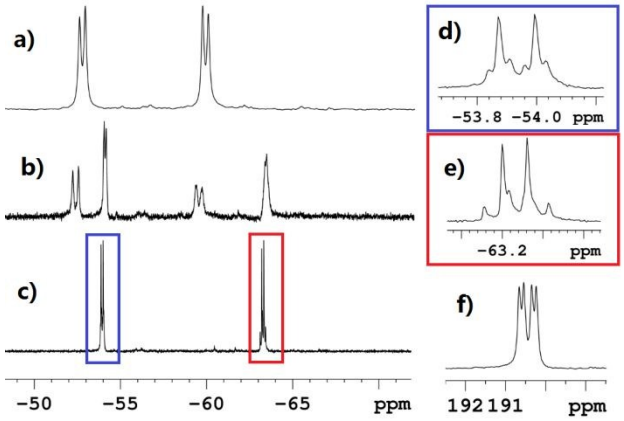

Fig. 7 Key NMR signals seen during the selective formation of **9e** when **1e** reacts with ^{13}CO at 203 K. a) $^{31}P\{^1H\}$ signals of **1e**, b) effect of ^{13}CO addition, c) $^{31}P\{^1H\}$ signals of **9e**, d) and e) reflect expansions of the $^{31}P\{^1H\}$ signals of **9e** and show the additional ^{13}C couplings, f) $^{13}C\{^1H\}$ NMR peak of the CO ligand in **9e** showing the analogous ^{31}P couplings

Reactions of 1a-1e with ^{13}CO and H_2

We then set out to explore the reactions of **1a**-**1e** with CO and H_2. These studies will be presented using **1b** as the example, the corresponding reactions with **1a** and **1c** behaving in a similar manner with directly analogous species being detected. We use ^{13}CO to ensure that we break the dihydride ligand symmetry in order to ensure that there is a PHIP response from the $Ir(H)_2(^{13}CO)_2$ core in these reactions.[86]

The reaction of **1b** with a mixture of ^{13}CO/*p*-H_2 (1:2 ratio with a total pressure of 3 atm.) was followed by ^{1}H NMR spectroscopy at 295 K as detailed in Fig 8. The sample was initially cooled, prior to filling with gas and placing it into the spectrometer in order to restrict the reactions starting point. As shown in Fig. 8a, hydride ligand signals for $\mathbf{2b_A}$ and $\mathbf{2b_B}$ were detected with low intensity. A stronger PHIP enhanced hydride ligand signal appeared at δ –8.8, alongside two much weaker signals at δ –8.0 and δ –8.2. Furthermore, the formation of the hydrogenation products propene and propane was suppressed by the addition of CO.

These three hydride peaks are split by a single *cis* phosphine and arise from dihydrides with the predicted square planar *cis*, *cis*-$(Ir)(^{13}CO)_2(H)_2$ core and hence possess features that are consistent with the those of an $[AX]_2$ spin system. Based on the requirements of electron counting, a further anionic ligand such as an alkyl or acyl group is required. ^{13}C information was obtained via HMQC methods that showed that the δ –8.8 signal connects to a terminal carbonyl resonance at δ 174.0 and no acyl resonance. In contrast, the δ –8.2 signal correlated to two signals at δ 171.9 (terminal CO) and δ 210.3 (acyl) and the δ –8.0 signal correlated to two signals at δ 172.5 (terminal CO) and δ 208.7 (acyl) respectively.

Hence the latter two resonances belong to acyl complexes. We propose therefore that the signal at δ −8.8 arises from $Ir(H)_2(^{13}CO)_2(P(p\text{-tol})_3)(\eta^1\text{-}CH_2CH{=}CH_2)$ (**10b**) of Scheme 5 and Table 7. It can be formed by *p*-H_2 addition to the η^1-isomer of **5b** or after CO loss from **6b** or $P(p\text{-tol})_3$ loss from **9b**. The latter two resonances reflect different acyl species with the same core $Ir(H)_2(CO)_2(P(p\text{-tol})_3)(COR)$ structure that must differ according to the identity of the alkyl group R. We propose that they are due to **Ir**$(H)_2(^{13}CO)_2(P(p\text{-tol})_3)(COCH_2CH{=}CH_2)$ (**11b$_L$**) and **Ir**$(H)_2(^{13}CO)_2(P(p\text{-tol})_3)(COC(CH_3){=}CH_2)$ (**11b$_B$**). We note that the related complex, Ir(dppe)(CO)$(H)_2$(COEt), has been seen by Eisenberg and exhibits similar characteristics to these.[52]

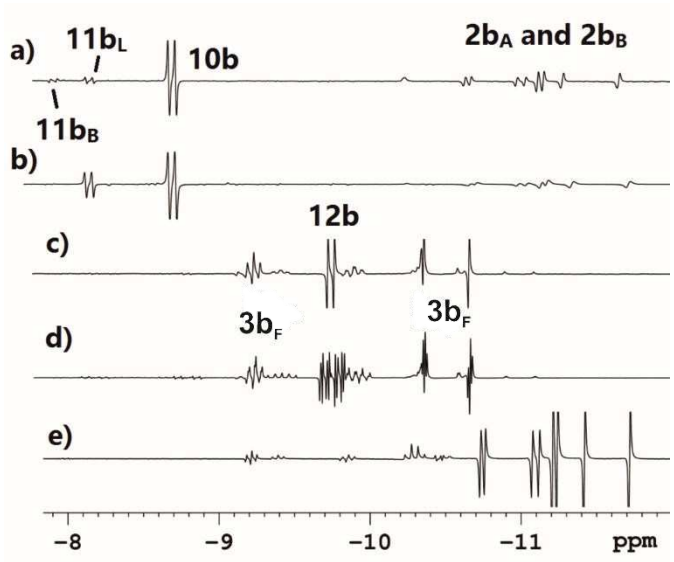

Fig. 8 Hydride region of a series of ^{1}H NMR spectra, (a)-(d), that were recorded at 295 K as **1b** reacts with *p*-H_2 and CO with resonances for the products **3b$_F$**, **10b**, **11b$_L$** and **11b$_B$** and **12b** indicated. a) $^1H\{^{31}P\}$ NMR trace, b) $^1H\{^{31}P\}$ NMR trace after a shake, c) $^1H\{^{31}P\}$ NMR trace at 315 K, d) corresponding ^{1}H NMR trace and e) corresponding $^1H\{^{31}P\}$ NMR trace without CO as a reference point.

One further important observation that lends support to these conclusions stems from the fact that PHIP enhanced signals are also seen in the organic region of these NMR spectra at δ 3.05 and δ 3.74 as shown in Fig. 10a. This figure details how complexes **10b** and **11b$_L$** yield an observable spin-spin coupling between their hydride resonances and a CH based signal. Both of the associated protons that give rise to these PHIP enhanced signals must originate in a single molecule of *p*-H_2 as they are connected by an antiphase H-H splitting in an analogous way to the inequivalent hydride ligands of **2b$_A$** and **2b$_B$** shown in Fig. 8a. They correspond to hydride and bound CH_2 proton signals (δ 3.05) in the η^1-allyl ligand of **10b** and hydride and acyl (δ 3.74) ligand signals in **11b**. A series of 1D EXSY experiments, where the hydride resonance of **10b** was selectively excited showed that although **10b** eliminates H_2, there is no exchange between the hydride and the site corresponding to the δ 3.05 signal. This confirms that the required hydride/CH_2 scrambling occurs prior to the formation of **10b**, most likely via the reversible generation of a labile propene hydride intermediate. This explanation also accounts for the act that propene itself shows weak PHIP in its ^{1}H NMR response as detailed earlier.

After several minutes in the spectrometer at 295 K, the enhanced hydride signal for **11b$_L$** grows in size relative to that of **11b$_B$** which almost disappears (Fig. 8b). However, upon taking the sample out of the spectrometer and repeating the shake process prior to re-observation, the ratio of the signal intensities for **10b** and **11b** change as the gas mixture is depleted.

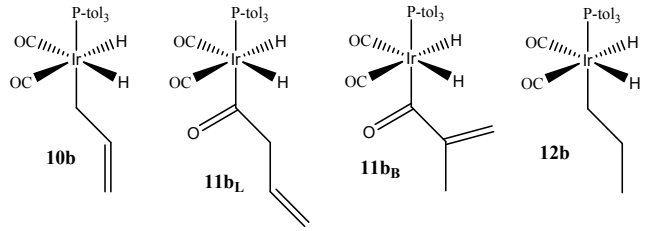

Fig. 9 Structures of **10b**, **11b$_L$**, **11b$_B$** and **12b** that are detected when **1b** reacts with CO and H_2 at 295 K.

Table 7 Multinuclear NMR data for the acyl and alkenyl dihydride complexes **10**, **11** and **12** that are detected with through a *p*-H_2 response at 295 K upon reaction of **1** with CO and *p*-H_2, couplings in Hz.

Species	^{1}H δ (multiplicity)	$^{13}C\{^1H\}$	$^{31}P\{^1H\}$
10a$_A$	−8.9 (2nd order, J_{HH} = 4, J_{PH} = 18)	173.7 (d, J_{PC} = 6 Hz, $CO_{terminal}$)	2.54 (s)
11a	−8.4 (2nd order, J_{HH} = 4, J_{PH} = 19)	171.6 (d, J_{PC} = 5, $CO_{terminal}$)	−8.4 (s)
		209.5 (dd, J_{PC} = 76, CO_{acyl})	
10b$_A$	−8.8 (2nd order, J_{HH} = 5, J_{PH} = 19)	174.0 (d, J_{PC} = 3, $CO_{terminal}$)	−8.22 (s)
11b	−8.2 (2nd order, J_{HH} = 5, J_{PH} = 19)	171.9 (d, J_{PC} = 4, $CO_{terminal}$)	−1.3 (s)
		210.3 (dd, J_{PC} = 78, CO_{acyl})	
10c$_A$	−9.2 (2nd order, J_{HH} = 5, J_{PH} = 20)	173.1 (d, J_{PC} = 5, $CO_{terminal}$)	−23.4 (s)
11c	−8.7 (2nd order, J_{HH} = 4, J_{PH} = 20)	170.9 (d, J_{PC} = 3, $CO_{terminal}$)	−30.7 (s)
		210.3 (dd, J_{PC} = 77, CO_{acyl})	
12e$_A$	−9.7 (m, $\lvert J_{P(trans)H} + J_{P(cis)H} \rvert$ = 104)	178.7 (d, J_{PC} = 5.0Hz, $CO_{terminal}$)	−47.5
12d$_A$	−9.7 (m, $\lvert J_{P(trans)H} + J_{P(cis)H} \rvert$ = 120)	-	−44.6
12d$_B$	−9.7 (m, J_{PH} = 122 and 20)	177.6 (d, J_{PC} = 5.0, $CO_{terminal}$)	−43.3
	−8.6 (m, J_{PH} = 20)		−52.5
10e$_A$	−9.6 (2nd order, J_{HH} = 4, J_{PH} = 22.8)	173.2 (d, J_{PC} = 4.8, $CO_{terminal}$)	−58.9 (s)
10e$_B$	−9.5 (dd, J_{HH} = -5, J_{PH} = 135.5)	172.6 ($CO_{terminal}$)	−60.4(s)
	−9.6 (dd, J_{HH} = -5, J_{PH} = 25.3)		

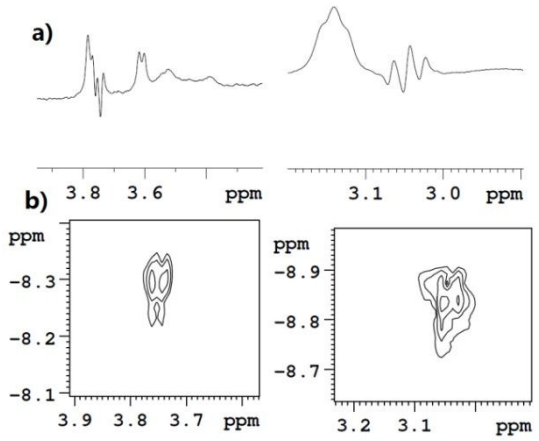

Fig. 10 a) Expansions of two ^{1}H NMR spectra showing how the PHIP effect is manifest in the Ir*CH*$_2$- and IrCO*CH*$_2$- signals of **10b** and **11b$_L$**, b) two ^{1}H-^{1}H COSY expansions which show correlations between these signals and the hydride ligand signals in these complexes to confirm these assignments.

When this sample is warmed to 315 K, a further dihydride signal began to appear at δ –9.80 which eventually became dominant. Its splitting pattern is very similar to that of **10b** and **11b**. 2D-HMQC experiments link this hydride signal to those of two ^{13}C centres, at δ 172.3 (terminal CO) and an acyl signal at δ 197.5, and a ^{31}P centre at δ –0.03 respectively. It is therefore likely to arise from the saturated acyl complex **12b** of Fig. 9 with the change in acyl chemical shift, relative to those of **11**, reflecting the change in saturation of the alkyl group.

The analogous reactions with complexes **1d** and **1e** were then examined, starting at 203 K. No new reactivity was seen until 263 K. At this point, with **1e**, a weak polarised hydride signal can be detected at δ –9.60 that has similar characteristics to those of **10b**. When this sample was warmed to 283 K, the signal for **10e$_A$** becomes much stronger (Fig. 11a), full characterisation data for **10e$_A$** is provided in ESI. A second set of hydride signals are detected at δ –9.48 (dd, J_{PH} = 135.5 Hz, J_{HH} = –5 Hz) and δ –9.60 (dd, J_{PH} = 25.3 Hz, J_{HH} = –5 Hz) due to a second isomer of Ir(H)$_2$(^{13}CO)$_2$(PMe$_3$)(η^1-CH$_2$CH=CH$_2$), **10e$_B$**. We note that although the hydride signals for **10e$_A$** and **10e$_B$** overlap they can be differentiated in a 2D ^{1}H-^{31}P HMQC measurement. We located partner ^{31}P signals at δ –59.0 for **10e$_A$** and at δ –60.4 for **10e$_B$** through this approach. **10e$_A$** and **10e$_B$** are expected to form from **1e** after ally ligand isomerisation and H_2 addition over the CO-Ir-CO axis or P-Ir-CH_2 axes respectively, a process which proceeds with a selectivity of 2:1. It is notable that PMe$_3$ loss from **9e** and CO loss from **6e** would lead to the same product.

The corresponding 283 K ^{1}H NMR spectrum also contains evidence for two further products. These reflect poorly enhanced hydride signals at δ –9.7 and δ –10.1 for the acyl complex Ir(H)$_2$(CO)(PMe$_3$)$_2$(CO-CH$_2$-CH=CH$_2$) (**12e**) and **3e$_A$** respectively. These complexes were identified on the basis of the corresponding ^{1}H NMR spectrum at 303 K (Fig. 11b). We note the signal at δ –9.68 linked to a proton signal at δ 3.88 (J_{HH} = 5 Hz and $J_{HH(hydride)}$ 1.4 Hz) in accordance with this.

Previously we saw that **3e$_A$** was stable at 298 K under H_2 but adding CO changes this situation and now **3e$_A$** transforms into **13e$_A$** at 303 K through ligand exchange and when this sample is warmed to 333 K, or kept at 303 K overnight, the acyl complex **Ir**(H)$_2$(CO)$_2$(PMe$_3$)(COCH$_2$CH=CH$_2$) (**13e$_A$**) dominates (Fig. 11d). We note **1d** proved to react in a similar fashion to **1e**. However, two isomers of the analogous acyl complex, **13d$_A$** and **13d$_B$**, are now produced in the ratio of 1.4:1. Neither **11e,** nor **11d** were seen in these studies**.**

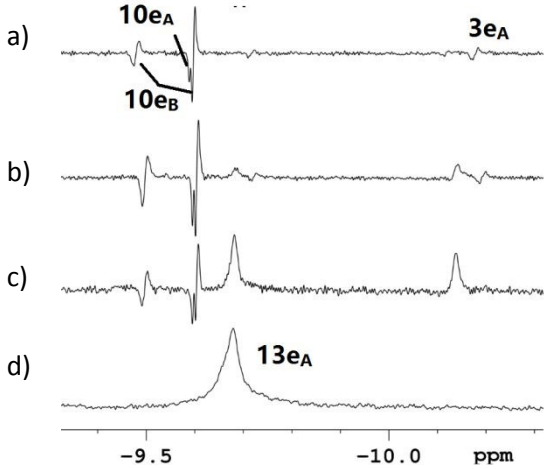

Fig. 11 Series of ^{1}H{^{31}P} NMR spectra showing how the signals in the hydride region change with temperature when the reaction of **1e**, H_2 and CO is followed. a) at 283 K, b) at 303 K, c) at 303 K, ca. one hour later and d) at 333 K.

We conclude therefore that when the phosphine is PMe$_3$ or PMe$_2$Ph, the fragment Ir(H)$_2$(CO)(COCH$_2$CH=CH$_2$) is optimally stabilized by two phosphine ligands.

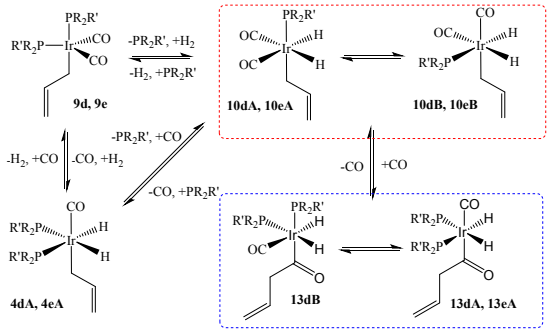

Scheme 5 Reaction pathways involving **9d**, **9e**, H_2 and CO

Conclusions

In conclusion we have demonstrated that the iridium allyl complexes Ir(CO)(PR$_2$R')$_2$(η^3-C$_3$H$_5$) (**1a**-**1e**) [where PR$_2$R' is PPh$_3$ (**1a**), P(*p*-tol)$_3$ (**1b**), PMePh$_2$ (**1c**), PMe$_2$Ph (**1d**) and PMe$_3$ (**1e**)] reflect suitable precursors to study the hydroformylation reaction in conjunction with *p*-H_2 as a range of reaction intermediates can be detected by PHIP assisted NMR spectroscopy. These products and their interconnectivity are illustrated in Scheme 6 and their detection serves to illustrate the successful mapping of the hydroformylation process. These studies have harnessed the differing reactivity conveyed by the phosphine variation to change the associated rates of reaction in

order to enable the efficient tracking of this process. Consequently, the identity of the phosphine can be concluded to play a significant role in controlling reactivity.

Reaction of **1** with *p*-H_2 at low temperatures typically revealed the formation of two isomers of the η^3-allyl dihydride species $Ir(H)_2(PR_2R')(CO)(\eta^3\text{-}C_3H_5)$ which is formed by phosphine loss. This reaction is favoured for electron rich phosphines such as PMe_3 and upon warming further reactions yield propene and propane alongside *fac* and *mer* isomers of $Ir(H)_3(CO)(PR_2R')_2$. Upon reaction with CO alone, equilibria are established between species such as $Ir(CO)_2(PPh_3)(\eta^3\text{-}C_3H_5)$, $Ir(\eta^1\text{-}C_3H_5)(CO)_3(PPh_3)$, $Ir(COCH_2CH{=}CH_2)(CO)_2(PPh_3)_2$ and $Ir(COCH_2CH{=}CH_2)(CO)_3(PPh_3)$ that confirm CO insertion into an Ir-C bond is possible. This reactivity results in the suppression of alkene hydrogenation when a mixture of CO and H_2 is examined and species such as *cis-cis* $Ir(COCH_2CHCH_2)(H)_2(CO)(PR_2R')$ and *cis-cis* $Ir(H)_2(\eta^1\text{-}C_3H_5)(CO)_2(PR_2R')$ are detected. These products subsequently eliminate C_4-aldehydes on warming to 318 K. Collectively the products detected here therefore map the hydroformylation mechanism for an iridium monohydride based catalyst as shown in Scheme 6. Given the ability of these systems to undergo CO and phosphine loss, roles for mono phosphine dicarbonyl and bisphosphine mono carbonyl intermediates are evident.

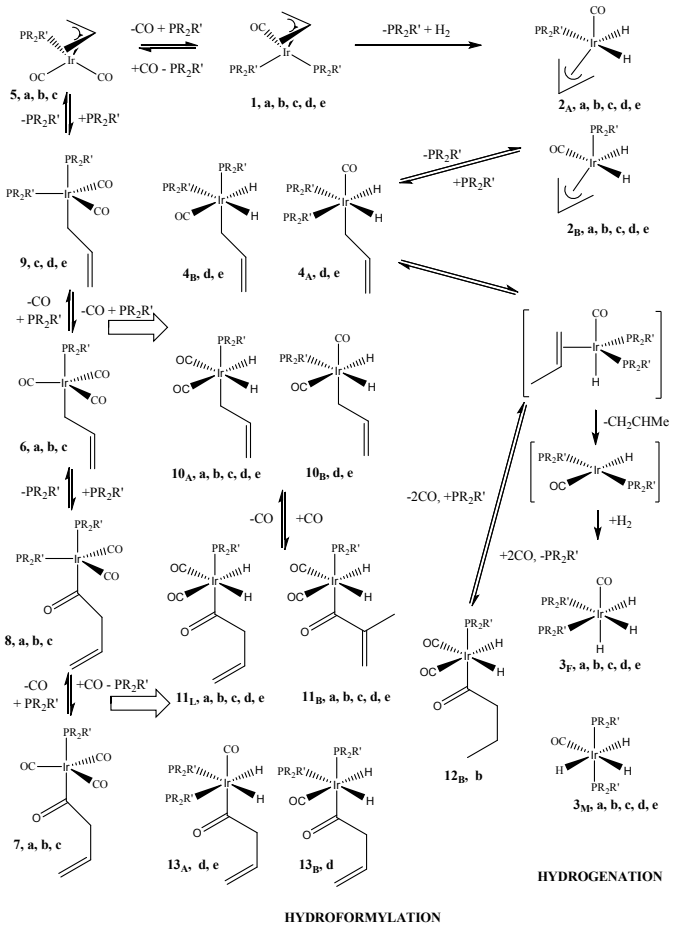

Scheme 6 Reaction pathways observed through the PHIP effect during the conversion of **1** into **3** by H_2 and CO

Acknowledgements

We are grateful for financial support from the China Scholarship Council for Dr Dexin Guan, the Wild Fund and SASOL.

View Article Online
DOI: 10.1039/C8DT04723E

Notes and references

1. S. Schmidt, E. Baráth, C. Larcher, T. Rosendahl and P. Hofmann, *Organomet.*, 2015, **34**, 841-847.
2. J. M. Birbeck, A. Haynes, H. Adams, L. Damoense and S. Otto, *ACS Catalysis*, 2012, **2**, 2512-2523.
3. O. Diebolt, H. Tricas, Z. Freixa and P. W. N. M. van Leeuwen, *ACS Catalysis*, 2013, **3**, 128-137.
4. R. M. Deshpande, Purwanto, H. Delmas and R. V. Chaudhari, *Ind. Eng. Chem. Res.*, 1996, **35**, 3927-3933.
5. C. K. Brown, W. Mowat, G. Yagupsky and G. Wilkinson, *J. Chem. Soc. A. Inorg. Phys. Theor.*, 1971, 850-859.
6. J. M. Brown and A. G. Kent, *J. Chem. Soc. Per.*, 1987, 1597-1607.
7. R. Tannenbaum and G. Bor, *J. Phys. Chem. A.*, 2004, **108**, 7105-7111.
8. M. R. Panman, J. Vos, V. Bocokić, R. Bellini, B. de Bruin, J. H. N. Reek and S. Woutersen, *Inorg. Chem.*, 2013, **52**, 14294-14298.
9. C. H. Beierlein, B. Breit, R. A. Paz Schmidt and D. A. Plattner, *Organomet.*, 2010, **29**, 2521-2532.
10. S. M. Massick, J. G. Rabor, S. Elbers, J. Marhenke, S. Bernhard, J. R. Schoonover and P. C. Ford, *Inorg. Chem.*, 2000, **39**, 3098-3106.
11. M. Diéguez, C. Claver, A. M. Masdeu-Bultó, A. Ruiz, P. W. N. M. van Leeuwen and G. C. Schoemaker, *Organomet.*, 1999, **18**, 2107-2115.
12. U. Gellrich, T. Koslowski and B. Breit, *Cat. Sci. Tech.*, 2015, **5**, 129-133.
13. L. E. Rush, P. G. Pringle and J. N. Harvey, *Angew. Chem. Int. Ed.*, 2014, **53**, 8672-8676.
14. T. Kegl, *RSC Advances*, 2015, **5**, 4304-4327.
15. Z. Tom and V. Louis, in *Homogeneous Transition Metal Catalyzed Reactions*, American Chemical Society, 1992, vol. 230, ch. 5, pp. 75-93.
16. S. Maeda and K. Morokuma, *J. Chem. Theory Comput.*, 2012, **8**, 380-385.
17. G. Alagona and C. Ghio, *J. Phys. Chem. A.*, 2015, **119**, 5117-5133.
18. C.-F. Huo, Y.-W. Li, M. Beller and H. Jiao, *Organomet.*, 2004, **23**, 765-773.
19. S. Schmidt, P. Deglmann and P. Hofmann, *ACS Catalysis*, 2014, **4**, 3593-3604.
20. C. Bianchini, H. M. Lee, A. Meli and F. Vizza, *Organomet.*, 2000, **19**, 849-853.
21. M. J. Chen, R. J. Klingler, J. W. Rathke and K. W. Kramarz, *Organomet.*, 2004, **23**, 2701-2707.
22. C. Dwyer, H. Assumption, J. Coetzee, C. Crause, L. Damoense and M. Kirk, *Coord. Chem. Rev.*, 2004, **248**, 653-669.
23. C. Godard, S. B. Duckett, C. Henry, S. Polas, R. Toose and A. C. Whitwood, *Chem. Commun.*, 2004, 1826-1827.
24. C. Godard, S. B. Duckett, S. Polas, R. Tooze and A. C. Whitwood, *Dalt. Trans.*, 2009, 2496-2509.
25. O. Diebolt, P. W. N. M. van Leeuwen and P. C. J. Kamer, *ACS Catalysis*, 2012, **2**, 2357-2370.
26. I. del Rio, W. G. J. de Lange, P. W. N. M. van Leeuwen and C. Claver, *Dalt. Trans.*, 2001, 1293-1300.

27. J. M. Manfred, in *High-Energy Processes in Organometallic Chemistry*, American Chemical Society, 1987, vol. 333, ch. 9, pp. 139-154.
28. S. M. Massick, T. Büttner and P. C. Ford, *Inorg. Chem.*, 2003, **42**, 575-580.
29. G. M. Torres, R. Frauenlob, R. Franke and A. Borner, *Cat. Sci. Tech.*, 2015, **5**, 34-54.
30. I. Fleischer, K. M. Dyballa, R. Jennerjahn, R. Jackstell, R. Franke, A. Spannenberg and M. Beller, *Angew. Chem. Int. Ed.*, 2013, **52**, 2949-2953.
31. H. W. Bohnen and B. Cornils, *Advances in Catalysis, Vol 47*, 2002, **47**, 1-64.
32. R. Franke, D. Selent and A. Borner, *Chem. Rev.*, 2012, **112**, 5675-5732.
33. A. Börner and R. Franke, *Hydroformylation Fundamentals, Processes, and Applications in Organic Synthesis*, Wiley-VCH Verlag GmbH & Co. KGaA, 2016.
34. P. W. N. M. van Leeuwen, *Rhodium Catalyzed Hydroformylation*, Springer Netherlands, Dordrecht, 2002.
35. J. P. Salinas-Olvera, R. M. Gómez and F. Cortés-Guzmán, *J. Phys. Chem. A.*, 2008, **112**, 2906-2912.
36. C.-F. Huo, Y.-W. Li, M. Beller and H. Jiao, *Organomet.*, 2003, **22**, 4665-4677.
37. P. N. Bungu and S. Otto, *Dalton Trans.*, 2011, **40**, 9238-9249.
38. W. Dong, J. Liu, H. Zhu, Y. Ding, Y. Pei, J. Liu, H. Du, M. Jiang, T. Liu, H. Su and W. Li, *J. Phys. Chem. C.*, 2014, **118**, 19114-19122.
39. F. Hebrard and P. Kalck, *Chem. Rev.*, 2009, **109**, 4272-4282.
40. L. Damoense, M. Datt, M. Green and C. Steenkamp, *Coord. Chem. Rev.*, 2004, **248**, 2393-2407.
41. S. A. Decker and T. R. Cundari, *New J. Chem.*, 2002, **26**, 129-135.
42. L. A. van der Veen, M. D. K. Boele, F. R. Bregman, P. C. J. Kamer, P. W. N. M. van Leeuwen, K. Goubitz, J. Fraanje, H. Schenk and C. Bo, *J. Am. Chem. Soc.*, 1998, **120**, 11616-11626.
43. Z. Freixa and P. W. N. M. van Leeuwen, *Dalton Trans.*, 2003, 1890-1901.
44. J. Pospech, I. Fleischer, R. Franke, S. Buchholz and M. Beller, *Angew. Chem., Int. Ed.*, 2013, **52**, 2852-2872.
45. I. Piras, R. Jennerjahn, R. Jackstell, A. Spannenberg, R. Franke and M. Beller, *Angew. Chem. Int. Ed.*, 2011, **50**, 280-284.
46. D. Hess, B. Hannebauer, M. Konig, M. Reckers, S. Buchholz and R. Franke, *Z.Naturforsch.(B)*, 2012, **67**, 1061-1069.
47. M. A. Moreno, M. Haukka and T. A. Pakkanen, *J. Catal.*, 2003, **215**, 326-331.
48. E. R. Nelsen and C. R. Landis, *J. Am. Chem. Soc.*, 2013, **135**, 9636-9639.
49. E. R. Nelsen, A. C. Brezny and C. R. Landis, *J. Am. Chem. Soc.*, 2015, **137**, 14208-14219.
50. G. Abkai, S. Schmidt, T. Rosendahl, F. Rominger and P. Hofmann, *Organomet.*, 2014, **33**, 3212-3214.
51. D. J. Fox, S. B. Duckett, C. Flaschenriem, W. W. Brennessel, J. Schneider, A. Gunay and R. Eisenberg, *Inorg. Chem.*, 2006, **45**, 7197-7209.
52. A. B. Permin and R. Eisenberg, *J. Am. Chem. Soc.*, 2002, **124**, 12406-12407.
53. S. B. Duckett and R. E. Mewis, *Acc. Chem. Res.*, 2012, **45**, 1247-1257.
54. J. López-Serrano, S. B. Duckett, S. Aiken, K. O. Almeida Leñero, E. Drent, J. P. Dunne, D. Konya and A. C. Whitwood, *J. Am. Chem. Soc.*, 2007, **129**, 6513-6527.
55. C. Godard, S. B. Duckett, S. Polas, R. Tooze and A. C. Whitwood, *J. Am. Chem. Soc.*, 2005, **127**, 4994-4995.
56. S. B. Duckett, G. K. Barlow, M. G. Partridge and B. A. Messerle, *J. Chem. Soc., Dalton Trans.*, 1995, 3427-3429.
57. S. Gloggler, A. M. Grunfeld, Y. N. Ertas, J. McCormick, S. Wagner and L. S. Bouchard, *Chem. Commun.*, 2016, **52**, 605-608.
58. S. Abdulhussain, H. Breitzke, T. Ratajczyk, A. Grunberg, M. Srour, D. Arnaut, H. Weidler, U. Kunz, H. J. Kleebe, U. Bommerich, J. Bernarding, T. Gutmann and G. Buntkowsky, *Chem. Eur. J.*, 2014, **20**, 1159-1166.
59. K. V. Kovtunov, I. E. Beck, V. V. Zhivonitko, D. A. Barskiy, V. I. Bukhtiyarov and I. V. Koptyug, *Phys. Chem. Chem. Phys.*, 2012, **14**, 11008-11014.
60. A. M. Balu, S. B. Duckett and R. Luque, *Dalt.Trans.*, 2009, 5074-5076.
61. I. V. Koptyug, K. V. Kovtunov, S. R. Burt, M. S. Anwar, C. Hilty, S. I. Han, A. Pines and R. Z. Sagdeev, *J. Am. Chem. Soc.*, 2007, **129**, 5580-5586.
62. V. V. Zhivonitko, V. V. Telkki, K. Chernichenko, T. Repo, M. Leskela, V. Sumerin and I. V. Koptyug, *J. Am. Chem. Soc.*, 2014, **136**, 598-601.
63. V. V. Zhivonitko, K. Sorochkina, K. Chernichenko, B. Kotai, T. Foldes, I. Papai, V. V. Telkki, T. Repo and I. Koptyug, *Phys. Chem. Chem. Phys.*, 2016, **18**, 27784-27795.
64. L. E. Longobardi, C. A. Russell, M. Green, N. S. Townsend, K. Wang, A. J. Holmes, S. B. Duckett, J. E. McGrady and D. W. Stephan, *J. Am. Chem. Soc.*, 2014, **136**, 13453-13457.
65. O. G. Salnikov, D. B. Burueva, D. A. Barskiy, G. A. Bukhtiyarova, K. V. Kovtunov and I. V. Koptyug, *ChemCatChem*, 2015, **7**, 3508-3512.
66. C. R. Bowers and D. P. Weitekamp, *J. Am. Chem. Soc.*, 1987, **109**, 5541-5542.
67. M. G. Pravica and D. P. Weitekamp, *Chem. Phys. Let.*, 1988, **145**, 255-258.
68. T. C. Eisenschmid, R. U. Kirss, P. P. Deutsch, S. I. Hommeltoft, R. Eisenberg, J. Bargon, R. G. Lawler and A. L. Balch, *J. Am. Chem. Soc.*, 1987, **109**, 8089-8091.
69. S. B. Duckett, C. L. Newell and R. Eisenberg, *J. Am. Chem. Soc.*, 1994, **116**, 10548-10556.
70. J. Barkemeyer, M. Haake and J. Bargon, *J. Am. Chem. Soc.*, 1995, **117**, 2927-2928.
71. J. Bargon, J. Kandels and P. Kating, *J. Chem. Phys.*, 1993, **98**, 6150-6153.
72. S. B. Duckett and R. E. Mewis, *Accounts Chem. Res.*, 2012, **45**, 1247-1257.
73. R. A. Green, R. W. Adams, S. B. Duckett, R. E. Mewis, D. C. Williamson and G. G. R. Green, *Prog. Nucl. Magn. Reson. Spectrosc.*, 2012, **67**, 1-48.
74. S. Gloggler, J. Colell and S. Appelt, *J. Magn. Reson.*, 2013, **235**, 130-142.
75. J. P. Collman and J. W. Kang, *J. Am. Chem. Soc.*, 1967, **89**, 844-851.
76. M. J. Burk and R. H. Crabtree, *Inorg. Chem.*, 1986, **25**, 931-932.
77. L. D. Field, E. T. Lawrenz and A. J. Ward, *Polyhedron*, 1999, **18**, 3031-3034.
78. K. D. John, K. V. Salazar, B. L. Scott, R. T. Baker and A. P. Sattelberger, *Chem. Commun.*, 2000, 581-582.

View Article Online
DOI: 10.1039/C8DT04723E

79. A. Sivaramakrishna, E. Hager, F. Zheng, H. Su, G. S. Smith and J. R. Moss, *J. Organomet. Chem.*, 2007, **692**, 5125-5132.
80. S. Biswas, Z. Huang, Y. Choliy, D. Y. Wang, M. Brookhart, K. Krogh-Jespersen and A. S. Goldman, *J. Am. Chem. Soc.*, 2012, **134**, 13276-13295.
81. K. Osakada, M. Kimura and J.-C. Choi, *J. Organo. Met.*, 2000, **602**, 144-150.
82. C. A. Tolman, *Chem. Rev.*, 1977, **77**, 313-348.
83. C. A. Tolman, *J. Am. Chem. Soc.*, 1970, **92**, 2953-2956.
84. A. L. Sargent and M. B. Hall, *Inorg. Chem.*, 1992, **31**, 317-321.
85. C. Kubis, W. Baumann, E. Barsch, D. Selent, M. Sawall, R. Ludwig, K. Neymeyr, D. Hess, R. Franke and A. Börner, *ACS Catalysis*, 2014, **4**, 2097-2108.
86. O. Torres, B. Procacci, M. E. Halse, R. W. Adams, D. Blazina, S. B. Duckett, B. Eguillor, R. A. Green, R. N. Perutz and D. C. Williamson, *J. Am. Chem. Soc.*, 2014, **136**, 10124-10131.

View Article Online
DOI: 10.1039/C8DT04723E

View Article Online
DOI: 10.1039/C8DT04723E

.

View Article Online
DOI: 10.1039/C8DT04723E

TOC

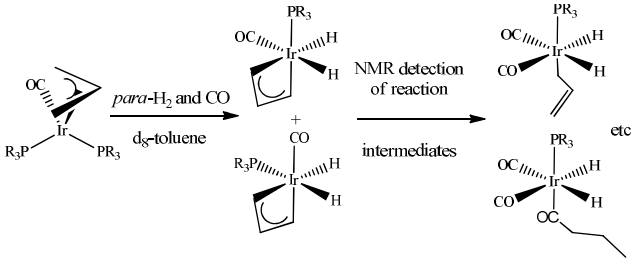

Para-hydrogen assisted NMR spectroscopy allows the detection of an array of reaction intermediates during iridium catalyzed hydroformylation